Catalysis Today 182 (2012) 46–53

Contents lists available at SciVerse ScienceDirect

Catalysis Today

journal homepage: www.elsevier.com/locate/cattod

Electroless deposition of ultrathin Au film for surface enhanced *in situ* spectroelectrochemisrty and reaction-driven surface reconstruction for oxygen reduction reaction

De-Jun Chen[a,b], Bolian Xu[a,c], Shi-Gang Sun[b,*], YuYe J. Tong[a,*]

[a] Department of Chemistry, Georgetown University, 37th & O Streets, NW, Washington, DC 20057, USA
[b] State Key Laboratory of Physical Chemistry of Solid Surfaces, College of Chemistry and Chemical Engineering, Xiamen University, Xiamen 361005, China
[c] Key Laboratory of Mesoscopic Chemistry of MOE, School of Chemistry and Chemical Engineering, Nanjing University, 22 Hankou Road, Nanjing 210093, Jiangsu, China

ARTICLE INFO

Article history:
Received 31 May 2011
Received in revised form 4 August 2011
Accepted 4 August 2011
Available online 12 October 2011

Keywords:
Au film electrode
Electroless deposition
SERS
In situ EC ATR-SEIRAS
ORR
Surface reconstruction

ABSTRACT

We report an investigation of the formation mechanism of a gold (Au) thin-film electrode made by electroless deposition for *in situ* electrochemical (EC) attenuated-total-reflection surface enhanced infrared adsorption spectroscopy (ATR-SEIRAS). The Au thin film was generated via galvanic electroless deposition from $[Au(S_2O_3)_2]^{3-}$ precursor and consisted of ~46 nm Au nanoparticles (NPs) deposited on Si infrared window. The observation of ν(Au–S) (263 cm^{-1}) and ν(S–S) (454 cm^{-1}) on the freshly deposited Au film using surface enhanced Raman spectroscopy (SERS) confirmed that the initial adsorbed sulfur species was $S_2O_3^{2-}$. Subsequent acid-treatment broke the S–S bond and yielded Au surface-bound atomic sulfur species. EC stripping of them led to the formation of (bi)sulfate identifiable by *in situ* EC ATR-SEIRAS. A sulfur coverage of 0.5 was estimated. We also discovered that square-wave treatment of the Au film led to significant surface reconstruction and much enhanced oxygen reduction reaction (ORR) activity. We attribute the latter to the reconstruction-caused new sites that could stabilize better the adsorbed ORR intermediates for facilitating the subsequent reaction step(s).

1. Introduction

Surface enhanced spectroscopic methods, such as surface enhanced Raman spectroscopy (SERS) and attenuated-total-reflection surface enhanced infrared adsorption spectroscopy (ATR-SEIRAS), are powerful techniques to study carbon monoxide oxidation reaction (COR) [1–4] and oxygen reduction reaction (ORR) [5–9]. Making high quality film electrode with high surface enhancement effect [10–12] is critical to revealing reaction mechanism in these studies by identifying reaction intermediates [4,6–8], e.g., surface water [13–15] and anion adsorption [1,16,17] during reaction, and their bonding configurations. Using adsorbed CO (CO_{ad}) as molecular probe is a classical text-book example of the latter by which active sites and components on catalyst surface can be discerned [1,18–20].

In terms of making Au thin films for *in situ* spectroelectrochemistry, electroless chemical deposition on Si infrared window from $[Au(S_2O_3)_2]^{3-}$ [21] possesses several advantages over electrochemical (EC) [22] or vacuum deposition [10,16]: (i) it is a faster and easier method; (ii) it avoids hydrocarbon contaminants; (iii) it shows a stronger surface enhancement effect; and (iv) it produces films that are of good electrical conductivity and also more stable. However, Au thin film formation mechanism as well as surface enhancement effect is still very much lacking so the use of the method has largely been an art rather than a science [11,12]. One objective of this paper is to obtain mechanistic information on the process of Au thin film formation at a molecular level. Once the Au film will be made, we will use oxygen reduction reaction (ORR) as a case study to advance our understanding of its structural ramifications.

2. Experimental

2.1. Electroless deposition of ultrathin Au film

Ultrathin (~tens nm) Au film electrode was electrolessly deposited onto a well-polished (equal edge) triangular Si prism (20 mm × 25 mm) optical window for ATR-SEIRAS [21]. The Si prism was first polished with successively finer grade alumina slurries down to 0.3 μm and cleaned by sonication in the Milli-Q water, followed by immersing one of the square surfaces in 5% NH_4F solution for several minutes to etch the surface. The etching process generated a hydrophobic surface. 1.5 mL plating solution, made

* Corresponding authors. Tel.: +1 202 687 5872; fax: +1 202 687 5591.
E-mail addresses: sgsun@xmu.edu.cn (S.-G. Sun), yyt@georgetown.edu (Y.Y.J. Tong).

0920-5861/$ – see front matter © 2011 Elsevier B.V. All rights reserved.
doi:10.1016/j.cattod.2011.08.052

by mixing 0.5 mL of $NaAuCl_4$ (15 mM) solution, 0.5 mL of Na_2SO_3 (150 mM), $Na_2S_2O_3$ (50 mM), and NH_4Cl (50 mM) mixture solution, and 0.5 mL of HF (0.4 mM) solution, was quickly injected all at once onto the Si surface that was pre-heated to 60 °C. After 90 s of plating, the plated surface was washed with copious ultrapure water and air-dried by Ar gas, which was the *as-freshly deposited (AFD) Au film*. In order to obtain the homogenous Au film reproducibly, fresh plating solution has to be used each time on a well-cleaned, hydrophobically etched Si surface under temperature control with ±1 °C accuracy.

The size of nanoparticles and surface morphology of the Au film electrodes were examined by field emission scanning electron microscopy (FE-SEM) (Zeiss SUPRA55-VP, 20 kV, Carl Zeiss Inc., Germany).

2.2. Raman spectroscopy

The SERS spectra were obtained using a confocal microprobe Raman system (Renishaw RM1000) equipped with a deep depletion CCD peltier cooled down to −70 °C. The microscope attachment is based on an Olympus BH2-UMA system and uses a 50× objective. A holographic notch filter was used to filter the excitation line, and 1200 g mm^{-1} selective holographic grating was employed depending on the spectral resolution required. The excitation wavelength was 785 nm from a Renishaw diode laser with a maximum power of 27 mW.

2.3. In situ EC ATR-SEIRAS

All EC SEIRAS data acquisitions were carried out on a Bruker Vector-22 Fourier transform IR spectrometer equipped with a liquid-nitrogen-cooled mercury–cadmium–telluride (MCT) detector. A home-made EC-IR cell with a triangular Si prism and an optical reflection accessory (incident angle of >60° enabling total attenuation reflection) was used for *in situ* measurements. The spectral resolution was 4 cm^{-1}. The obtained spectra were shown in the absorbance units defined as $-\log(I/I_0)$ where I and I_0 are the singe-beam spectral intensities at the measuring potential and the reference potential, respectively.

All EC experiments were carried out in a conventional three-electrode EC-IR cell using a CHI-660D potentiostat. Large surface-area Pt gauze and Ag/AgCl (3 M) (Bioanalytical) were used as counter and reference electrodes, respectively. We had the *AFD Au film* treated by 0.1 M $HClO_4$ (GFS chemicals, 70%, Cl < 0.1 ppm) for 1 h (denoted as *acid-treated Au film*), following by subjecting the Au film to repeated potential cycling between −0.2 V and 1.4 V at 50 mV/s until a stable cyclic voltammogram (CV) was reached (denoted as *CV-treated Au film*). *In situ* EC ATR-SEIRAS was also applied to monitor this stripping process on another *acid-treated Au film* while stair-step potentials were carried out. ORR was carried out on the CV-treated Au surface with O_2-bubbling (ultra-high purity oxygen, GTS·Welco, 99.993%, THC < 1 ppm) solution. For meaningful comparison, the speed of bubbling was maintained during CVs acquisition. Square-wave (SW) potentials between 0.3 V and 1.2 V at 50 Hz were applied to reconstruct active Au surface in an O_2-saturated solution. All electrode potentials in this paper were cited with respect to the Ag/AgCl (3 M) reference electrode. All solutions were prepared using 18.2 MΩ cm Milli-Q water with ultralow organic impurity (TOC < 2 ppb).

3. Results and discussion

3.1. Electroless deposition of Au film electrode

A proper Au film electrode needs to be generated for *in situ* SEIRAS or SERS spectroscopic studies of surface-bound adsorbates [10]. It has been shown that galvanic electroless deposition produced better metal films (for instance Au [21], Cu [23], or Pt [24]) on Si prism in terms of electric conductivity and film stability than by EC deposition [22]. Alternatively, Cai's group succeeded in chemical deposition of Cu [25], Ag [26], Pt, Pd, and Pt–Pd alloy [27] films on Si based on seeded growth method which does not require the subsequent dissolution of Si. Furthermore, the size and shape of NPs can be well controlled by using properly chosen surfactant(s). In our electroless deposition of Au film, metal NPs were deposited onto pre-treated Si surface from $[Au(S_2O_3)_2]^{3-}$ precursor in a colorless plating solution by displacing Si in HF solution.

Fig. 1a and b shows the low and high magnification SEM images of the AFD Au film on the Si prism. As can be seen in Fig. 1a, Au film was continuous and covered the entire surface of the Si substrate. This ensured good electrical conductivity required for good SEM images and EC studies. The high magnification image (Fig. 1b) reveals that the film actually consisted of compact Au NPs with average size of 46 nm (inset in Fig. 1a). This value is consistent with observations reported in earlier papers [21,28]. This size of NPs is expected to show excellent SEIRAS properties [10], which is illustrated by the inset in Fig. 1b that shows the SEIRAS of CO_{ad} at 0.0 V whose intensities are 0.016 and 0.007 abs for atop and bridge-bonding CO_{ad} respectively. Such signal intensity is much higher than that of traditional IRAS [10,29].

Notice that a CO IR band at about 2107 cm^{-1} was observed when the electrolyte was saturated with gaseous CO, as reported previously. But it disappeared once the gaseous CO was cleaned from the solution. The two bands at 2052 and 1875 cm^{-1} shown in the inset of Fig. 1b were very stable and remained unchanged even after the solution was cleaned from the gaseous CO. Despite similar vibrational frequencies, it is highly unlikely though that they were caused by Pt contamination for the following reasons. First, we used highly pure chemicals free of Pt to prepare the deposition solution. Second, there were no any indications of the presence of Pt in the CVs (see Fig. 1c). Third, we measured EDX on the deposited Au film on the Si prism and no Pt was detected. Thus, we believe that these two bands belong to strongly adsorbed linear- and bridge-CO on the highly rough Au surface.

Fig. 1c shows the 1st (blue) and 2nd (red) CVs of the Au film in 0.1 M deoxygenated $HClO_4$ solution. Clearly, adsorbate generated from $S_2O_3^{2-}$ was stripped away in the 1st cycle as compared to the 2nd one. The latter resembles a typical Au CV profile [30–32]. As clearly shown in the inset, Fig. 1c, the surface was almost completely blocked by the adsorbates during the 1st cycle (blue) but was fully recovered during the 2nd cycle (red), suggesting that one cycle stripping was enough to clean the Au film surface off the adsorbates. The 2nd CV profile is similar to those of single crystal planes of (1 0 0) terrace with abundant steps, such as (3 1 0) or (2 1 0) [31]. The first gold oxidation peak in the 2nd cycle can be assigned to (1 1 0) sites [30]. That this oxidation has the highest current indicates that the adsorbate-stripping may have created many local (1 1 0) domains on the NPs surface, probably due to Au atoms' rearrangement. Remarkably, the ratio of the oxidation charge of the adsorbates to that of reduction of Au surface oxide (Fig. 1c, blue) is always ~2.5 (2.54–2.58) on five different *acid-treated Au films*, which indicates a stable stoichiometric number of adsorbate to exposed surface Au atoms.

To identify the adsorbate, we employed SERS to track surface reactants as shown in Fig. 2c–e. As references, we also show in Fig. 2a and b the Raman spectra of solid and solution $Na_2S_2O_3$ respectively. By comparison, we assign the Raman band at 454 cm^{-1} to ν(S–S) of the adsorbed $S_2O_3^{2-}$ [33] whose vibration frequency is only blue-shifted 6 cm^{-1} with respect to the corresponding band of the $Na_2S_2O_3$ solution (Fig. 2b), but 21 cm^{-1} to that of $Na_2S_2O_3$ solid (Fig. 2a). Such comparison demonstrates clearly that $S_2O_3^{2-}$ still remained the major species adsorbed on

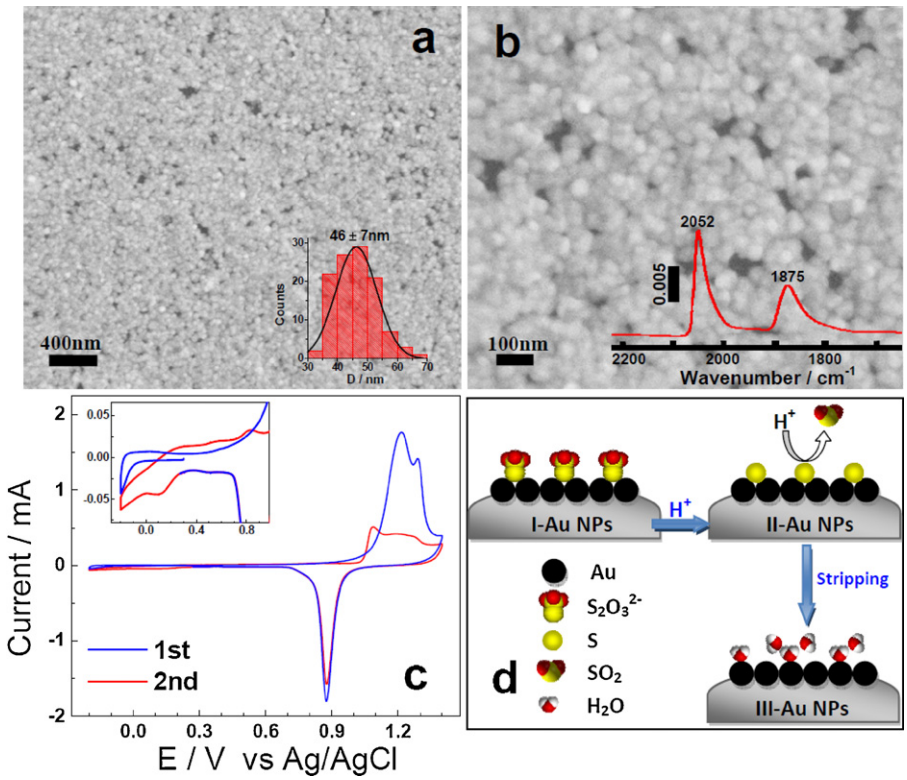

Fig. 1. SEM images of *the AFD Au film* electrode in low (a) and high (b) magnifications. The inset in (a) shows the size distribution of Au NPs and that in (b) the surface enhanced IR bands of adsorbed CO at 0 V referenced to the spectrum recorded at 1 V, respectively. (c) The 1st (blue) and 2nd (red) CVs of *AFD Au film* electrode in 0.1 M $HClO_4$; the inset shows enlarged view in low potential region. (d) The schematic illustration of electroless deposition mechanism of Au film and stripping of surface capped reactant. (For interpretation of the references to color in this figure legend, the reader is referred to the web version of the article.)

the Au surface and could not be removed simply by washing and that this adsorbate is likely to adsorb individually in monolayer due to steric hindrance of adsorbed molecules. Additionally, the appearance of the ν(Au–S) band at 263 cm^{-1} with a shoulder around 300 cm^{-1} [34,35] indicates that the $S_2O_3^{2-}$ bound to the *AFD* Au film through the lone sulfur. Another important observation is that no Raman bands corresponding to ν_{syn}(S=O) (996 cm^{-1}) and δ_{syn}(S=O) (668 cm^{-1}) were observed in SERS spectra of the $S_2O_3^{2-}$ on *AFD* Au film (Fig. 2c). This might be attributed to the Raman inactiveness of the S=O bonding due to bonding orientation. By using the surface selection rules [36–38], we hypothesize that thiosulfate anions were vertically adsorbed to the Au surface as illustrated in Fig. 1d-I. On the other hand, surface enhancement effect for SERS enabled the ν(Au–S) vibration band to be observed for $S_2O_3^{2-}$ adsorbed on ~46 nm Au NPs [34,35,39] while no such band was observed in our 5 mM $[Au(S_2O_3)_2]^{3-}$ plating solution.

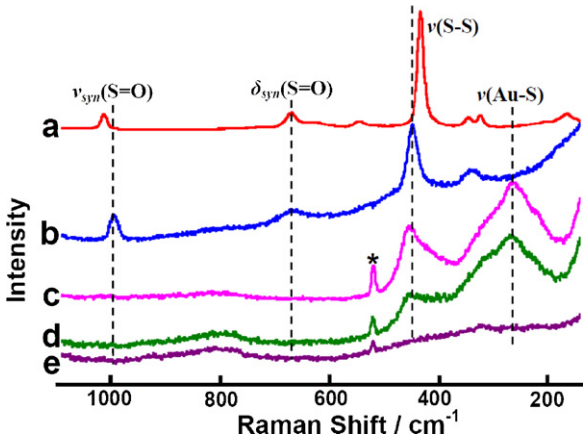

Fig. 2. Raman spectra of solid $Na_2S_2O_3$ (a), 0.5 M $Na_2S_2O_3$ solution (b); and SERS of *the AFD Au film* (c), the *acid-treated Au film* (d) and the *CV-treated Au film* (e). * indicates peaks from Si prism. All spectra have no potential control.

The intensity of the ν(S–S) vibrational band was dramatically decreased after immersing the Au film in acid for 1 hr. This indicates that acid-washing of the Au film may disintegrate the adsorbed $S_2O_3^{2-}$, in agreement with the well-known instability of $S_2O_3^{2-}$ in acidic environment [40]. However, the residual band at 463 cm^{-1} (Fig. 1d) could not be eliminated even by immersing the Au film in acid for 12 h. Its intensity only decreased by further electro-oxidation, similar to our previous studies of sulfur adsorption on Pt [41,42]. We hypothesize that this persisting band at 463 cm^{-1} might be due to adsorbed S atoms generated during the disintegration of $S_2O_3^{2-}$. That is, acid-immersion broke the S–S bond as illustrated in Fig. 1d-II, which can be rationalized by the well-known reaction of thiosulfate decomposition in acid [43,44]: $Au\text{–}S_2O_3^{2-} + 2H^+ \rightarrow Au\text{–}S + SO_2 + H_2O$. No simultaneous appearance of bands at 460 cm^{-1} and 218 cm^{-1} was observed, which is the spectroscopic signature of poly sulfur for ν(S–S) and δ(S–S–S), respectively, on Au surface [34,35,39,45].

What is surprising is that the band at 263 cm^{-1} assigned to ν(Au–S) of adsorbed $S_2O_3^{2-}$ also persisted, contradicting apparently to the assumed disintegration of adsorbed $S_2O_3^{2-}$. This can be attributed to no significant change of the Au–S bonding during disintegration and suggests that the chemical state of the lone S of adsorbed $S_2O_3^{2-}$ resembles elemental sulfur when it bonds to the Au surface. After CV stripping, all bands disappeared (Fig. 2e), suggesting that stripping can eliminate effectively the adsorbed sulfur-containing species (S_{ad}). This is consistent with the observation that the open-circuit potential (OCP) increased from 0.14 V pre-CV stripping to 0.42 V post CV stripping.

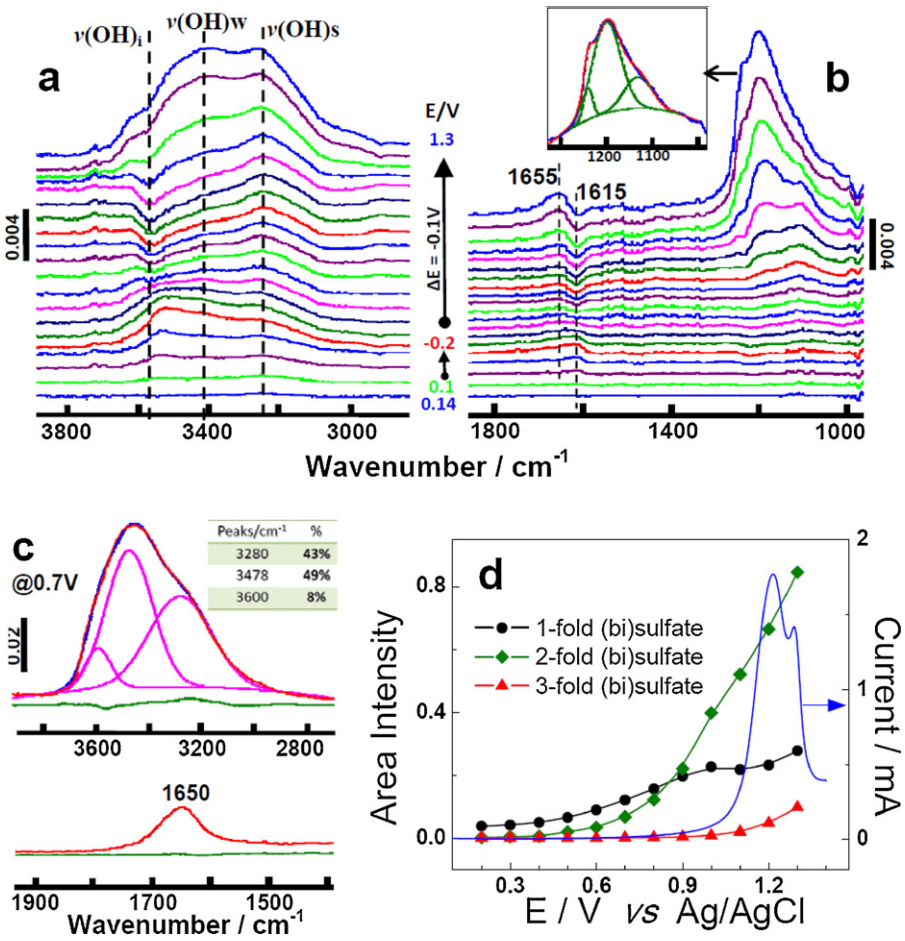

Fig. 3. The potential dependence of ATR-SEIRAS spectra on the *acid-treated Au film* in (a) 3000–3800 cm^{-1} and (b) 1000–1800 cm^{-1} spectral regions; the inset in (b) shows three deconvoluted bands of the adsorbed 1-, 2-, and 3-fold (bi)sulfate for products of adsorbate oxidation at 1.3 V. (c) The comparison of surface water species before (green) and after (red) stripping at 0.7 V. The pink line shows the three deconvoluted water bands whose percentage ratios are presented in the inset table; (d) the corresponding potential dependent band (integral) intensities of the three types adsorbed (bi)sulfate in (b) produced during the adsorbate oxidation on *the acid-treated Au film*. (For interpretation of the references to color in this figure legend, the reader is referred to the web version of the article.)

To identify the final product for S_{ad} oxidation on the *AFD* Au film, we carried out *in situ* EC ATR-SEIRAS study of the Au film. The step potentials were applied from the OCP, 0.14 V, to −0.2 V then to 1.3 V as indicated in Fig. 3a and b. Three SEIRAS bands at ~1100, ~1185 and ~1240 cm^{-1} were observed. They overlaps with IR bands that have been attributed to the ν(S=O) vibrations of sulfate (SO_4^{2-}) or bisulfate (HSO_4^-) [29,46,47]: 1-, 2-, and 3-fold (bi)sulfate adsorption respectively via 1, 2 or 3 oxygen atoms on Pt [48–50] or Au [45,51]. But despite these extensive experimental studies, the assignments of these bands are still under debates. With these uncertainties in mind, we adopted the assignments of the 1-, 2-, and 3-fold (bi)sulfate on Pt NPs reported in Ref. [48], that is, assigning the IR bands at ~1100, ~1185 and ~1240 cm^{-1} to 1-, 2-, and 3-fold (bi)sulfate adsorptions on Au NPs respectively, for two main reasons. The first is that the Pt NPs studied in Ref. [48] and the Au NPs investigated here have very similar particle size and packing morphology as revealed by the respective SEM images. The second is that rather detailed and reasonable discussions on peak position and assignment, electrode potential sensitivity, and stark effect were provided for the triple IR bands observed on Pt NPs.

The potential dependence of integrated intensities for these bands is plotted in Fig. 3d. As can be seen, the onset potential for the 1- and 2-fold (bi)sulfate formation coincides with that of the stripping CV (inset in Fig. 1c), i.e., ~0.5 V. But the 3-fold one only appeared at potential above 1.0 V where the major oxidation peak locates. Notice that the peak area of the 1- or 2-fold (bi)sulfate is still much larger than that of the 3-fold one at the height of the oxidation peak. Since the 3-fold coordination adsorption is less likely to happen on Au(1 0 0) surface [50,51], the dominant presence of the 2-fold (bi)sulfate adsorption indicates a corresponding dominant (1 0 0) orientation of the *AFD* Au film that consisted of ~ 46 nm Au NPs (*vide infra*). Thus, the sulfur coverage calculated by the stable ratio of oxidation and reduction charges (Fig. 1c, blue) is 0.50 ($\theta_{S_{ad}}$ = 0.50), in agreement with the value (0.52) obtained on Au(1 0 0) in vacuum [52]: $(2e^{-*}1Au + 6e^{-*}\theta_S)/(2e^{-*}1Au) = 2.5 \rightarrow \theta_S = 0.5$.

The interaction of water with solid surface is fundamentally important in surface chemistry [14,53,54]. Since the pioneering work of Osawa on ATR-SEIRAS [16], many interesting studies [13,15,18,55] have revealed hydrogen-bonded network of water in solid–liquid interface for catalysis in electrochemistry, thanks to the higher surface sensitivity of ATR-SERAIS [10,16]. It has been proposed [15,16,18,55] that there are three types of water at the interface for hydrogen-bonded water network: strongly hydrogen-bonded ice-like water ($\nu(OH)_s$, Fig. 1d-III middle), disordered weakly hydrogen-bonded water ($\nu(OH)_w$, Fig. 1d-III right) and isolated non-hydrogen-bonded water ($\nu(OH)_i$, Fig. 1d-III left) at 3000–3250, ~3400 and ~3600 cm^{-1}, respectively. As shown in Fig. 3a, the three ν(OH) vibrational bands were identifiable at 3255, 3408, and 3570 cm^{-1} for $\nu(OH)_s$, $\nu(OH)_w$ and $\nu(OH)_i$ respectively.

Interestingly, the largest intensity change with potential sweeping (0.14 → −0.2 → 0.5 V) was observed for the isolated water at 3570 cm^{-1} on S-covered Au surface. Its intensity increased with

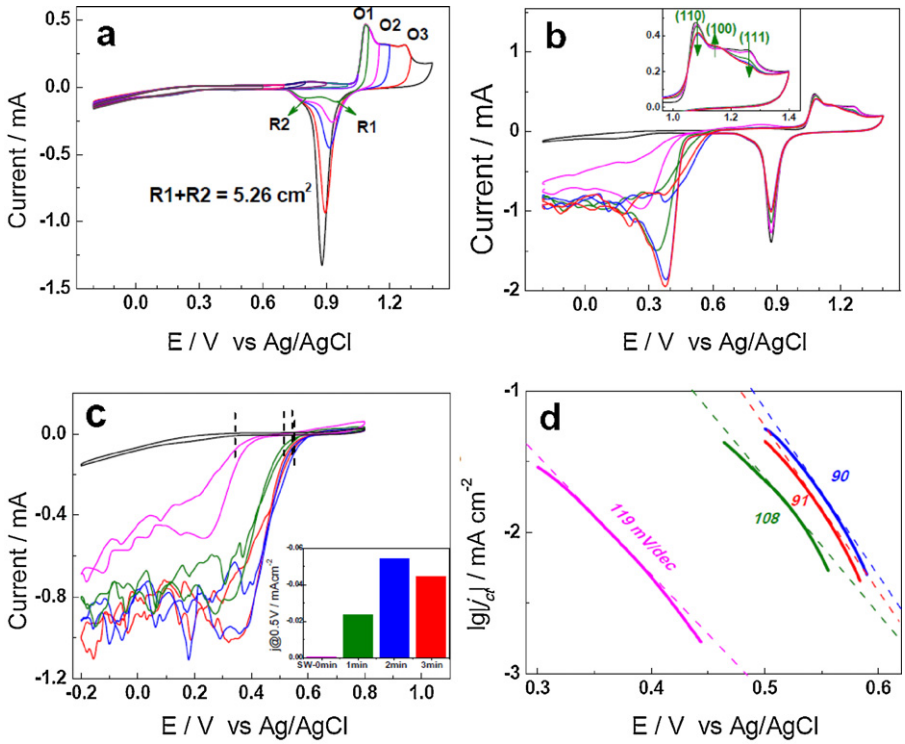

Fig. 4. (a) Cyclic voltammetry of *CV-treated Au film* electrode with different high limited potentials in Ar-saturated 0.1 M $HClO_4$ at 50 mV/s; (b) CVs between −0.2 and 1.4 V at 50 mV/s in O_2-saturated solution; (c) CVs between −0.2 and 0.8 V at 20 mV/s after the square-wave (SW) treatment (0.3/1.2 V, 50 Hz) was applied on Au film for 0 min (pink), 1 min (green), 2 min (blue) and 3 min (red) respectively. The inset in (b) zooms into Au surface oxidation peaks on SW-treated films except the black line is CV in Ar-saturated solution and the inset in (c) is the bar-representation of the specific current densities measured at 0.5 V (d) Tafel curve analysis for anodic scanning and the inset shows the ORR activities for anodic current at 0.5 V as a function of the SW treatments (same color). (For interpretation of the references to color in this figure legend, the reader is referred to the web version of the article.)

cathodic scanning (CS) but decreased with anodic scanning (AS), which coincided perfectly with the variation in the bending vibration δ(HOH) at 1615 cm^{-1} (Fig. 3b). This synchronization enabled us to identify the vibration position of δ(HOH) for the isolated water on Au surface, which is quite lower than the vibrational frequency of other types of adsorbed water (*vide infra*). Since the isolated adsorbed water was generally observed on surface where other adsorbates, such as CO [13,15,55] or O [16,18] occupied most of sites, the observation of it indicates a high coverage of S_{ad} on the *AFD* Au film. Above 1.0 V, the amount of all three types of adsorbed water increased because of the oxidation of S_{ad}. Remarkably, the intensity of water vibrational bands (Fig. 3c, red) recorded at 0.7 V after the complete oxidation of S_{ad} was ~20 times stronger than that at the same potential on S_{ad}-covered surface (Fig. 3c, green). The deconvolution of the band (pink) showed that the integral percentage ratio of the isolated water was about 8% as compared to 43% for the strongly hydrogen-bonded ice-like water and 49% for the disordered weakly hydrogen-bonded water. However, the real amounts of these adsorbed waters cannot be determined due to the H-bonding dependent intensity enhancement in IR absorption which is unknown. Concomitantly, the bending vibration of δ(HOH) was at 1650 cm^{-1}, which is 35 cm^{-1} higher than that of isolated water at 1615 cm^{-1} (Fig. 3b).

3.2. ORR on the Au film electrode

Once the Au film electrode was made, we proceeded ahead to investigate ORR on it. Fig. 4a shows the stable CVs of the *CV-treated Au film* with increasing up-potential limit. These CV profiles were highly reproducible, suggesting that we had clean and stable Au surface for the subsequent ORR study. Based on EC studies of the well-defined Au single crystal surfaces [30,31,56], we assigned the sharp anodic peaks at 1.08 V (O1) and 1.28 V (O3) to oxidation of Au(1 1 0) and Au(1 1 1) domains respectively and the peak in between (O2) to oxidation of Au(1 0 0) domain. When the up-limiting potential was set to just above the O1 peak, two reduction peaks for the Au(1 1 0) oxides appeared (green CV in Fig. 4a): 0.95 V (R1) and 0.81 V (R2). As the up-limiting potential increased incrementally, the R1 peak intensity increased with peak potential negatively shifted but the R2 peak showed only minor changes. The latter indicates that the R2 is uniquely associated with the reduction of the Au(1 1 0) domain oxide (O1). The total surface area of the Au film, 5.26 cm^2, was estimated using the reduction charge of the CV with the highest up-limiting potential (Fig. 4a, black) [57]. Dividing this value by the geometric area in direct contact with electrolyte gave a roughness factor of 3.4.

For ORR on the Au film in O_2-saturated 0.1 M $HClO_4$ (Fig. 4b, pink), the onset potential was 0.44 V (0.7 V vs. RHE in 0.1 M $HClO_4$) which is identical to values reported previously in acid solution [56,58,59]. The oxidation peaks of Au(1 1 0), Au(1 0 0) and Au(1 1 1) (pink curve in the inset of Fig. 4b) are almost identical to those of the blank CV of the CV-treated Au film in Ar-saturated solution (black curve in the inset). Interestingly, the ORR activity was substantially enhanced after subjecting the CV-treated Au film to an additional treatment of square-wave potentials (0.3 V/1.2 V, 50 Hz) in O_2-saturated solution for up to 3 min. They were denoted as Au-SW1 (green), Au-SW2 (blue) and Au-SW3 (red) for 1, 2 or 3 min respectively in Fig. 4b–d and the original one without any SW treatment (black) as Au-SW0.

For CS returning from an up-limiting potential of 1.4 V, the onset potential for ORR was almost the same for all surfaces: 0.48 V (Fig. 4b). But the reduction current increased much more sharply for the SW-treated surfaces than non-treated one that let to an apparent positive shift of the half-wave potential, although all of them

reached comparable diffusion controlled current after going over a peak current which was surface-treatment dependent. As to the subsequent AS, there was also a clear positive shift of the half-wave potential of the ORR for the SW-treated Au surfaces (Fig. 4b) among which the Au-SW2 (blue curve) registered the largest positive shift (0.14 V) as compared to the non-treated one (pink curve), indicating the highest ORR activity. But no current peaks were observed.

More interesting is that ORR current was observed at potential region positive to the onset potential (0.48 V) of the CS, i.e., in potential region where no ORR current was observed for the latter. Furthermore, if the up-limiting potential was set to 0.8 V, the above-observed large peak current during the CS almost disappeared and the AS current curves overlapped with the corresponding CS curves (Fig. 4c). This indicates that the large current peaks observed in Fig. 4b were not due to ORR (*vide infra*). As a comparison, the specific current densities at 0.5 V for the ASs shown in the inset of Fig. 4c (0.023, 0.054 and 0.044 mA cm^{-2} for Au-SW1, Au-SW2, and Au-SW3 respectively) were plotted in bar figure as an inset in Fig. 4c. No ORR current was observed for Au-SW0 at 0.5 V. Again, the Au-SW2 showed highest ORR activity.

To gain more insight into the observed ORR activity enhancement by the SW treatments of the Au film electrode, Tafel curve and slope [59–61] of the AS curves (Fig. 4c) are shown in Fig. 4d for analyzing the kinetics of the ORR. Tafel slopes were calculated in the kinetic control regimes as indicated by the vertical dotted lines in Fig. 4c. The corresponding Tafel slope of ORR on the Au-SW0 was 119 mV/dec, suggesting that the first electron transfer to O_2 molecule ($O_{2ad} + e^- \rightarrow {O_2}^-_{ad}$) was the rate determining step (RDS) [59–61]. With the SW treatments, the Tafel slopes dropped down to 108, 90 and 91 mV/dec for Au-SW1, Au-SW2 and Au-SW3, respectively. These observed changes in the Tafel slope imply changes in RDS. One possible new RDS could be simultaneous or sequential reduction and protonation of ${O_2}^-$ as discussed in previous experimental and theoretical studies [62–65]. Blizanac et al. [59] also observed the Tafel slope drop from 125 mV/dec in 0.1 M $HClO_4$ to 90 mV/dec in 0.1 M KOH on Au(1 0 0), which was attributed to the energetics of the Au(1 0 0)–${O_2}^-$ interaction and the availability of active sites for the adsorption of ${O_2}^-$ or other reaction intermediates.

It has been observed that the ORR kinetics can have strong dependence on both surface structure [56,59,66,67] and anion (or adsorbed OH) adsorption [58,68]. In our case, we measured Tafel slopes on slightly changed surface by SW treatments but in the same solution. We thus believed that the ORR kinetics change we observed was most likely a pure structure effect. As the inset of Fig. 4b shows, SW treatment decreased the Au(1 1 1) and Au(1 1 0) domains but left the Au(1 0 0) domain almost intact or even increased it slightly. At the same time, the reduction peaks of Au oxide at 0.88 V decreased gradually. We can glean further corroborating evidence of the structural effect by inspecting the *in situ* EC ATR-SEIRAS spectra shown in Fig. 5a and b. These spectra were recorded at 0.3 V and referenced to the one for Au-SW0. The band at 1228 cm^{-1} (Fig. 5b) can be assigned to 3-fold adsorption of ${ClO_4}^-$ anions similar to that of (bi)sulfate [48]. Its intensity decreased substantially as the time of SW treatment increased. It has been known that (1 1 1) surface favors 3-fold adsorption of ${ClO_4}^-$ anions but (1 0 0) surface does not due largely to the symmetric match between a tetrahedral anion and (1 1 1) surface [49,69]. Therefore, the decrease in band intensity at 1228 cm^{-1} with SW treatments is consistent with the CV observation indicating a decrease of the (1 1 1) domain.

On the other hand, the intensity of the band of strongly hydrogen bound water vibrating at ~3200 cm^{-1} increased while that of the weakly hydrogen bound water vibrating at ~3500 cm^{-1} decreased (Fig. 5a). Additional evidence of structural change comes from the SEM images of the Au thin film surface after SW treatment, as

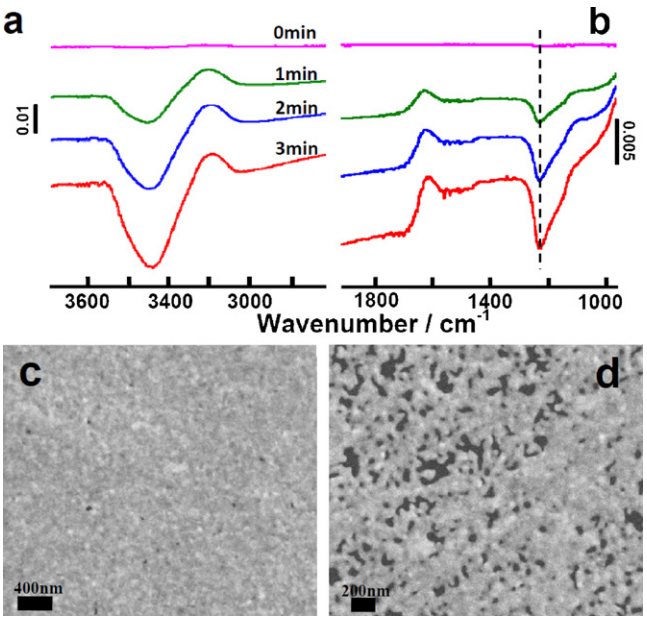

Fig. 5. ATR-SEIRAS spectra of the Au film treated by SW for 0 min (pink), 1 min (green), 2 min (blue) and 3 min (red) in 2800–3800 cm^{-1} (a) and 1000–1800 cm^{-1} (b) regions. All were taken at 0.3 V in O_2-satureted 0.1 M $HClO_4$ except that the reference spectrum was taken in Ar-saturated solution. SEM images (c and d) of Au film after treatment for 3 min. (For interpretation of the references to color in this figure legend, the reader is referred to the web version of the article.)

shown in Fig. 5c and d which should be compared to the images of Fig. 1a and b. As can be seen, the SW treatment caused significant surface reconstruction by "melting" all the NPs that homogenized the boundary of NPs and made the surface more like a continuous Au electrode surface. Yet evidence (inset in Fig. 4b) shows that the Au(1 0 0) domain somehow survived the SW treatment and was largely intact.

Fig. 6 shows the CV profiles on the Au-SW3 Au surface in Ar-saturated solution. Compared to the CV of the Au-SW0 (black), oxidation peaks of Au(1 1 0) and Au(1 1 1) domains (red) were much less pronounced on the Au-SW3. Consequently, the R2 (associated with the Au(1 1 0) domain, *vide supra*) and R1 (comparing red reduction peak with the black one) also decreased. On the other hand, a new reduction peak at 0.4 V (R3) appeared once the up-limiting potential was beyond 1 V and increased as the up-limiting potential increased. This indicates the appearance of a new type of surface sites that were different from those related to R1 and

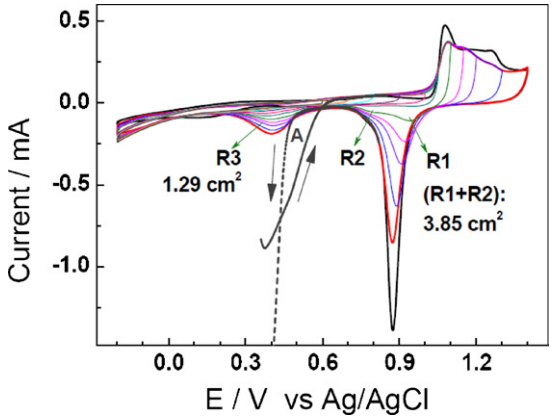

Fig. 6. CVs of SW-treated Au film in 0.1 M Ar-saturated $HClO_4$ with different high limited potentials at 50 mV/s. The black one is CV of original Au film. The dash dark line indicates the corresponding ORR curves.

R2 and growth at the expense of the latter two. The corresponding area R3 sites were about 1.29 cm^2, about a fourth of the total Au surface area (R1 + R2 + R3, 5.14 cm^2). The latter value is slightly smaller than that of the original total surface area of the Au-SW0 (black, R1 + R2, 5.26 cm^2), due probably to surface morphological changes (Fig. 5c and d).

What is interesting is that the onset of ORR for CS (dashed black line) overlapped with that of the reduction of the R3 species. This coincidence led us to speculate that the R3 sites created by the SW treatments were responsible for the observed ORR enhancement. When the up limiting potential goes beyond 1 V (for instance 1.4 V in Fig. 4b), the R3 sites starts to be oxidized and will not be active for ORR until they are reduced. Since the onset potential of the clean R3 sites for ORR was more positive than the onset potential of the reduction of their oxidized form (see the AS curves in Fig. 4b), the current is expected to increase steeply once the oxidized R3 sites are reduced in CS and will include contributions from both ORR and the reduction of the oxidized R3 sites. This explains the observed steeply rising current and the current peaks in Fig. 4b. In the AS, the R3 sites were free and their higher activity in ORR led to the observed ORR current in potential region positive to 0.48 V (dashed black line). However, the exact reason why the R3 sites are more active in ORR than the R1 and R2 sites is still unknown and is currently under investigation

4. Conclusions

We have reported in this paper that the electroless deposition from $[Au(S_2O_3)_2]^{3-}$ precursor produced a highly conductive and stable Au film electrode of tens nm thickness that consisted of ~46 nm Au NPs on the Si infrared window. We revealed the mechanistic information spectroscopically about the molecular processes of deposition in which Au(III) cations were reduced with the $S_2O_3^{2-}$ anions maintaining their molecular integrity and bound to the formed Au film via the lone sulfur atom. The ensuing acid treatment broke the S–S bonding of $S_2O_3^{2-}$ anions and yielded atomic sulfur and sulfide anions adsorbed on the Au film. The total sulfur coverage was estimated to be $\theta_{S_{ad}} = 0.50$, which could be completely removed by 1 cycle CV stripping up to 1.4 V. The ATR-SEIRAS study proved that the final product of the stripping was (bi)sulfate. Additionally, we were able to assign unambiguously the frequency of water bending vibration, 1615 cm^{-1}, to the isolated surface water species.

While similar ORR activity as polycrystalline Au in acid was observed on cleaned Au film electrode, square-wave potential treatment could enhance substantially its ORR activity. The half-wave potential registered a positive shift of about 0.14 V on the Au-SW2 (Fig. 4b). Tafel slope dropping from 119 to 90 mV/dec after SW treatment suggests a change in the RDS. We speculated that it could be a reaction step involved simultaneous or very rapid sequential reduction and protonation of $O_2^-{}_{ad}$. We found that the SW-treatment turned part of the Au(1 1 1) and Au(1 0 0) sites into a new type of sites designated as R3 sites as a result of surface reconstruction which accounted for about a quarter of the total sites (Fig. 6). Evidence suggests that they were responsible for the observed ORR activity enhancement. The mechanistic ramifications of the R3 sites are currently under investigation and we hope to report them in near future.

Acknowledgements

The authors are indebted to Mr. William Craig and Mr. Leon Der for their skillful assistance in trouble-shooting electronics and computers and in making the infrared reflection adaptor. De-Jun Chen is partially supported by a CSC (Chinese Scholar Council, 2009631048) graduate fellowship and Bolian Xu is a CSC-Georgetown post-doc fellow. The research in the Sun lab is supported by NSFC (20921120405, 21021002), and the research in the Tong lab is supported by NSF (CHE-0923910) and by DOE (DE-FG02-07ER15895).

References

[1] G. Samjeske, K. Komatsu, M. Osawa, The Journal of Physical Chemistry C 113 (2009) 10222.
[2] T. Sato, K. Kunimatsu, H. Uchida, M. Watanabe, Electrochimica Acta 53 (2007) 1265.
[3] H. Yang, Y. Yang, S. Zou, The Journal of Physical Chemistry C 111 (2007) 19058.
[4] A. Miki, S. Ye, M. Osawa, Chemical Communications 38 (2002) 1500.
[5] B.S. Yeo, S.L. Klaus, P.N. Ross, R.A. Mathies, A.T. Bell, ChemPhysChem 11 (2010) 1854.
[6] M.-h. Shao, P. Liu, R.R. Adzic, Journal of the American Chemical Society 128 (2006) 7408.
[7] M.H. Shao, R.R. Adzic, The Journal of Physical Chemistry B 109 (2005) 16563.
[8] X. Li, A.A. Gewirth, Journal of the American Chemical Society 127 (2005) 5252.
[9] X. Li, A.A. Gewirth, Journal of the American Chemical Society 125 (2003) 7086.
[10] M. Osawa, Diffraction and Spectroscopic Methods in Electrochemistry: In-situ Surface-enhanced Infrared Spectroscopy of the Electrode/Solution Interface, Wiley-VCH, New York, 2006.
[11] I. Zorić, M. Zäch, B. Kasemo, C. Langhammer, ACS Nano 5 (2011) 2535.
[12] Y. Yokota, K. Ueno, H. Misawa, Chemical Communications 47 (2011) 3505.
[13] M. Watanabe, T. Sato, K. Kunimatsu, H. Uchida, Electrochimica Acta 53 (2008) 6928.
[14] D. Menzel, Science 295 (2002) 58.
[15] M. Osawa, M. Tsushima, H. Mogami, G. Samjeske, A. Yamakata, The Journal of Physical Chemistry C 112 (2008) 4248.
[16] K.-i. Ataka, T. Yotsuyanagi, M. Osawa, The Journal of Physical Chemistry 100 (1996) 10664.
[17] J.-H. Ha, J. Kim, Chemical Physics Letters 502 (2011) 92.
[18] D.-J. Chen, A.M. Hofstead-Duffy, I.-S. Park, D.O. Atienza, C. Susut, S.-G. Sun, Y.J. Tong, The Journal of Physical Chemistry C 115 (2011) 8735.
[19] Yan, Q.-X. Li, S.-J. Huo, M. Ma, W.-B. Cai, M. Osawa, The Journal of Physical Chemistry B 109 (2005) 7900.
[20] T. Yajima, H. Uchida, M. Watanabe, The Journal of Physical Chemistry B 108 (2004) 2654.
[21] H. Miyake, S. Ye, M. Osawa, Electrochemistry Communications 4 (2002) 973.
[22] G. Oskam, et al., Journal of Physics D: Applied Physics 31 (1998) 1927.
[23] L.A. Nagahara, T. Ohmori, K. Hashimoto, A. Fujishima, Journal of Electroanalytical Chemistry 333 (1992) 363.
[24] M. Cerruti, G. Doerk, G. Hernandez, C. Carraro, R. Maboudian, Langmuir 26 (2010) 432.
[25] H.F. Wang, Y.G. Yan, S.J. Hu, W.B. Cai, Q.H. Xu, M. Osawa, Electrochimica Acta 52 (2007) 5950.
[26] S.J. Huo, X.K. Xue, Q.X. Li, S.F. Xu, W.B. Cai, The Journal of Physical Chemistry B 110 (2006) 25721.
[27] C. Wang, B. Peng, H.N. Xie, H.X. Zhang, F.F. Shi, W.B. Cai, The Journal of Physical Chemistry C 113 (2009) 13841.
[28] S.G. Sun, W.B. Cai, L.J. Wan, M. Osawa, The Journal of Physical Chemistry B 103 (1999) 2460.
[29] T. Iwasita, F.C. Nart, Progress in Surface Science 55 (1997) 271.
[30] A. Hamelin, Journal of Electroanalytical Chemistry 407 (1996) 1.
[31] A. Hamelin, A.M. Martins, Journal of Electroanalytical Chemistry 407 (1996) 13.
[32] B.B. Blizanac, M. Arenz, P.N. Ross, N.M. Markovic, Journal of the American Chemical Society 126 (2004) 10130.
[33] Z. Gabelica, Chemistry Letters 8 (1979) 1419.
[34] C. Quijada, F.J. Huerta, E. Morallon, J.L. Vazquez, L.E.A. Berlouis, Electrochimica Acta 45 (2000) 1847.
[35] X. Gao, Y. Zhang, M.J. Weaver, Langmuir 8 (1992) 668.
[36] C.L. Haynes, A.D. McFarland, R.P.V. Duyne, Analytical Chemistry 77 (2005) 338A.
[37] X. Gao, J.P. Davies, M.J. Weaver, The Journal of Physical Chemistry 94 (1990) 6858.
[38] M. Moskovits, J.S. Suh, The Journal of Physical Chemistry 88 (1984) 5526.
[39] P.G. Lustemberg, C. Vericat, G.A. Benitez, M.E. Vela, N. Tognalli, A. Fainstein, M.L. Martiarena, R.C. Salvarezza, The Journal of Physical Chemistry C 112 (2008) 11394.
[40] R. Steudel, T. Gobel, G. Holdt, Zeitschrift fur Naturforschung B 43 (1988) 203.
[41] I.-S. Park, B. Xu, D.O. Atienza, A.M. Hofstead-Duffy, T.C. Allison, Y.J. Tong, ChemPhysChem 12 (2011) 747.
[42] B. Xu, I.-S. Park, Y. Li, D.-J. Chen, Y.J. Tong, Journal of Electroanalytical Chemistry (2011), doi:10.1016/j.jelechem.2011.02.031.
[43] V.I. Gorokhovskaya, G.S. Vorobeva, Zhurnal Obshchei Khimii 55 (1985) 156.
[44] T. Loucka, Collection of Czechoslovak Chemical Communications 63 (1998) 20.
[45] M. Weber, F.C. Nart, Langmuir 12 (1996) 1895.
[46] M. Ito, Surface Science Reports 63 (2008) 329.
[47] A. Lachenwitzer, N. Li, J. Lipkowski, Journal of Electroanalytical Chemistry 532 (2002) 85.
[48] D.-M. Zeng, Y.-X. Jiang, Z.-Y. Zhou, Z.-F. Su, S.-G. Sun, Electrochimica Acta 55 (2010) 2065.
[49] N. Hoshi, A. Sakurada, S. Nakamura, S. Teruya, O. Koga, Y. Hori, The Journal of Physical Chemistry B 106 (2002) 1985.

[50] F.C. Nart, T. Iwasita, M. Weber, Electrochimica Acta 39 (1994) 2093.
[51] G.J. Edens, X. Gao, M.J. Weaver, Journal of Electroanalytical Chemistry 375 (1994) 357.
[52] M. Kostelitz, J.L. Domange, J. Oudar, Surface Science 34 (1973) 431.
[53] M.A. Henderson, Surface Science Reports 46 (2002) 1.
[54] H. Ogasawara, B. Brena, D. Nordlund, M. Nyberg, A. Pelmenschikov, L.G.M. Pettersson, A. Nilsson, Physical Review Letters 89 (2002) 276102.
[55] Y.-G. Yan, B. Peng, Y.-Y. Yang, W.-B. Cai, A. Bund, U. Stimming, The Journal of Physical Chemistry C 115 (2011) 5584.
[56] S. Strbac, R.R. Adzic, Journal of Electroanalytical Chemistry 403 (1996) 169.
[57] S. Trasatti, O.A. Petrii, Pure and Applied Chemistry 63 (1991) 711.
[58] S. Strbac, R.R. Adzic, Electrochimica Acta 41 (1996) 2903.
[59] B.B. Blizanac, C.A. Lucas, M.E. Gallagher, M. Arenz, P.N. Ross, N.M. Markovic, The Journal of Physical Chemistry B 108 (2004) 625.
[60] R.R. Adzic, S. Strbac, N. Anastasijevic, Materials Chemistry and Physics 22 (1989) 349.
[61] A. Sarapuu, K. Tammeveski, T.T. Tenno, V. Sammelselg, K. Kontturi, D.J. Schiffrin, Electrochemistry Communications 3 (2001) 446.
[62] A.J. Appleby, Journal of Electroanalytical Chemistry 357 (1993) 117.
[63] J.J. Warren, T.A. Tronic, J.M. Mayer, Chemical Reviews 110 (2010) 6961.
[64] J.A. Keith, G. Jerkiewicz, T. Jacob, ChemPhysChem 11 (2010) 2779.
[65] J.A. Keith, T. Jacob, Angewandte Chemie International Edition 49 (2010) 9521.
[66] J. Perez, H.M. Villullas, E.R. Gonzalez, Journal of Electroanalytical Chemistry 435 (1997) 179.
[67] N.M. Markovic, R.R. Adic, V.B. Vesovic, Journal of Electroanalytical Chemistry and Interfacial Electrochemistry 165 (1984) 121.
[68] J.X. Wang, N.M. Markovic, R.R. Adzic, The Journal of Physical Chemistry B 108 (2004) 4127.
[69] A.M. Funtikov, U. Stimming, R. Vogel, Journal of Electroanalytical Chemistry 428 (1997) 147.